Naturally, there is still much time spent preparing and isolating the chromosomal DNA. This remains a major bottleneck on the way to mapping the entire human genome.

REFERENCES

(1) Andrew, L.; Olson, M. V. *Genetics* **1991**, *127*, 681-698.
(2) Jordan, E. *Anal. Chem.* **1991**, *63*, 420A-423A.
(3) Drossman, H.; Luckey, J. A.; Kostichka, A. J.; D'Cunha, J.; Smith, L. M. *Anal. Chem.* **1990**, *62*, 900-903.
(4) Schwartz, D. C.; Cantor, C. R. *Cell* **1984**, *37*, 67-75.
(5) Schwartz, D. C. In *New Directions in Electrophoretic Methods*; Jorgenson, J. W., Phillips, M., Eds.; ACS Symposium Series 335; American Chemical Society: Washington, DC, 1987; pp 167-181.
(6) Lai, E.; Birren, B. W.; Clark, S. M.; Simon, M. I.; Hood, L. *Biotechniques* **1989**, *7* (1), 34-42.
(7) Chu, G.; Vollrath, D.; Davis, R. W. *Science* **1986**, *234*, 1582-1585.
(8) Lalande, M.; Noolandi, J.; Turmel, C.; Rousseau, J.; Slater, G. W. *Proc. Natl. Acad. Sci. U.S.A.* **1987**, *84*, 8011-8015.
(9) Vlovy, J. L. *Biopolymers* **1987**, *26*, 1929-1940.
(10) Deutsch, J. M. *Science* **1988**, *240*, 922-924.
(11) Olson, M. V. *J. Chromatogr.* **1989**, *470*, 377-383.
(12) de la Cruz, M. O.; Gersappe, D.; Schaffer, E. O. *Phys. Rev. Lett.* **1990**, *64*, 2324-2327.
(13) Chan, K. C.; Koutny, L. B.; Yeung, E. S. *Anal. Chem.* **1991**, *63*, 746-750.
(14) Chu, G.; Vollrath, D.; Davis, R. Personal communication, Stanford University Medical Center, 1987.
(15) Dawkins, H. J. S. *J. Chromatogr.* **1989**, *492*, 615-639.
(16) Lewis, E. M.; Kouri, R. E.; Latorra, D.; Berka, K. M.; Lee, H. C.; Gaensslen, R. E. *J. Forensic Sci.* **1990**, *35*, 1186-1190.
(17) Fritsch, E. F.; Maniatis, T. *Molecular Cloning: A Laboratory Manual*, 2nd ed.; Cold Spring Harbor Laboratory Press: New York, 1989; p B.23.
(18) Woolley, P. *Electrophoresis* **1987**, *8*, 339-345.
(19) Noolandi, J.; Rousseau, J.; Slater, G. W.; Turmel, C.; Lalande, M. *Phys. Rev. Lett.* **1987**, *58*, 2428-2431.
(20) Ulanovsky, L.; Drouin, G.; Gilbert, W. *Nature* **1990**, *343*, 190-192.
(21) Pattee, P. A. *Genet. Maps* **1990**, *5*, 2.22-2.27.
(22) Hung, L. C.; Bandziulis, R. *Promega Notes* **1990**, *24*, 1-3.
(23) Pattee, P. A. In *The Bacterial Chromosome*; Drlica, K., Riley, M., Eds.; John Wiley and Sons; New York, 1990; pp 163-169.
(24) Burke, D. T. *Genet. Anal.: Techn. Appl.* **1990**, *7* (5), 94-99.
(25) Noolandi, J. *Makromol. Chem., Rapid Commun.* **1991**, *12*, 31-35.

RECEIVED for review July 15, 1991. Accepted October 3, 1991. The Ames Laboratory is operated by Iowa State University for the U.S. Department of Energy under Contract W-7405-Eng-82. This work was supported by the Director of Energy Research, Office of Health and Environmental Research.

Dual-Field and Flow-Programmed Lift Hyperlayer Field-Flow Fractionation

S. Kim Ratanathanawongs and J. Calvin Giddings*

Field-Flow Fractionation Research Center, Department of Chemistry, University of Utah, Salt Lake City, Utah 84112

Field and flow programming and their combination, dual programming, are shown to extend the particle size range to which a single flow/hyperlayer field-flow fractionation (FFF) run is applicable to ~1-50 μm. The rationale for programming flow/hyperlayer FFF (or other forms of lift hyperlayer FFF) is to expand the diameter range of micron size particles that can be resolved in a single run. By contrast, the reason for programming normal-mode FFF, the only kind of programming previously realized in FFF, is to reduce the analysis time of submicron particle samples of considerable size variability. These differences are explained in detail in relationship to the basic mechanisms governing retention in normal, steric, and lift hyperlayer FFF. Experiments are described in which field, flow, and dual programming are used to expand the accessible diameter range of flow/hyperlayer FFF. An example is shown in which 11 sizes of latex microspheres in the 2-48-μm diameter range are separated by dual programming in 11 min.

INTRODUCTION

In the time since the general concept of field-flow fractionation (FFF) was first presented in the 1960s (*1*), FFF has been developed into an effective tool for the separation and analysis of macromolecules, polymers, colloids, and fine particles (*2-9*). Many basic developments have led to the improvement of FFF in the intervening years. These improvements have included methods (e.g., steric FFF) that have enlarged the range of applicability of FFF, optimization strategies that have enhanced speed and resolution, and systems that have provided more versatile driving forces (e.g., cross flow) that are applicable to a broader class of complex materials.

One important improvement in FFF since its inception is that of programming. In *programmed FFF*, the field strength, the flow velocity, or some other retention-controlling parameter is varied in the course of a run, primarily for the purpose of speeding up the elution of slowly migrating components. The concept of programming in FFF was first developed and applied by Yang, Myers, and Giddings (*10*). However, this initial programming concept, along with all subsequent experimental programming work reported for FFF, has been applied only to the so-called normal mode of FFF operation (*11-19*). It is the object of this work to show that programming is not only applicable to, but highly effective with, another major operating mode of FFF termed hyperlayer FFF, particularly in the specific form termed lift hyperlayer FFF, a close relative of steric FFF. While a cursory analysis suggests that little would be gained by such an extension of programming techniques, a more thorough analysis provides a clear rationale for the programming of lift hyperlayer FFF. The rationale and the experimental evidence in its support are presented in this paper.

CONTRAST OF NORMAL AND HYPERLAYER MODE PROGRAMMING

In FFF the separation of macromolecular and particulate species is achieved by injecting a small sample containing the species into a stream of carrier fluid that flows lengthwise through a thin elongated channel (*2-9*). The primary driving force, generated by an externally controlled field or gradient, is applied transversely across the thin dimension of the channel in a direction perpendicular to flow. This driving force induces a transverse displacement of component species across the channel, generally toward one wall termed the accumulation wall. As the particles approach the wall, their overall motion is halted by one of several possible opposing forces

0003-2700/92/0364-0006$03.00/0

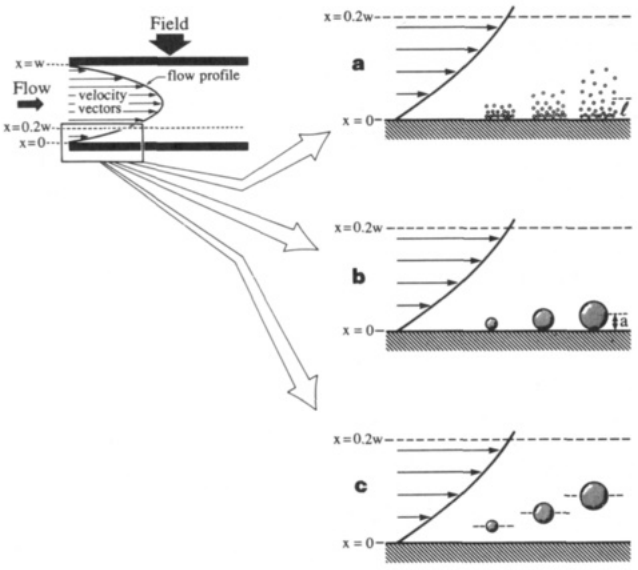

Figure 1. Separation mechanism in the (a) normal, (b) steric, and (c) hyperlayer modes of FFF.

or displacement effects. For one, the particles may diffuse back away from the wall. They may also be driven back from the wall by various repulsive forces. Because of these opposing influences and the thinness of the channel, each type of particle (or macromolecule) comes rapidly to equilibrium. The final equilibrium position or distribution across the thin dimension of the channel is determined by the balance of the primary driving force and the opposing forces (*8*, *20*, *21*). Different kinds or sizes of particles are subject to different forces and thus have different equilibrium positions or distributions.

More specifically, different kinds of opposing forces or effects lead to different mathematical forms of the equilibrium distribution of the sample particles and thus to what is known as different operating modes (*8*, *21*, *22*). When the opposing effect is dominated by diffusion, we have the *normal operating mode* of FFF. The term "normal" arises from the fact that this was the only operating mode utilized in field-flow fractionation until the advent of steric FFF, a second operating mode, in the late 1970s (*23*).

As the stream of carrier fluid flows through the channel, it carries the various particle types along with it. Most often the channel flow profile is parabolic or near-parabolic, which means that the velocity of flow is highest in the center of the channel and slowest near the wall (see Figure 1). With parabolic flow, any particle type whose equilibrium position is near a wall is carried only slowly down the channel by flow. A particle type whose equilibrium position is further removed from the nearest wall is displaced more rapidly by flow. Because flow displacement ("migration") velocities vary in this manner from one particle type to another, the different particle species are separated. The mechanism is illustrated in Figure 1.

In the normal mode of FFF, small particles almost invariably elute from the channel before large particles because small particles equilibrate at a relatively high mean elevation ℓ (on the x coordinate) above the accumulation wall (Figure 1a). Furthermore, the velocity of migration through the channel is approximately proportional to ℓ. Specifically, the retention ratio R, equal to the ratio of the particle migration velocity $\mathcal{V}$ to the mean fluid velocity $\langle v \rangle$ can be approximated by (*24*)

$$R = \mathcal{V}/\langle v \rangle = 6\ell/w \tag{1}$$

where w is the channel thickness. For a component to be retained, ℓ should be significantly less than $0.2w$. This mean elevation is given by

$$\ell = D/U \tag{2}$$

where D is the diffusion coefficient of the particles in the carrier fluid and U is the velocity of transverse displacement of particles toward the accumulation wall induced by the primary driving force. Small particles generally have larger D values and smaller U values than large particles. As a consequence, small particles have larger ℓ values and thus migrate more rapidly (have larger R values) than large particles. This is the *normal elution order*.

One of the general advantages of normal-mode FFF is that ℓ is very sensitive to particle diameter d or molecular weight M. For example in *sedimentation/normal FFF* (Sd/Nl FFF), an FFF subtechnique in which the primary driving force is sedimentation, U is proportional to d^2 and D is inversely proportional to d, causing ℓ to vary as $1/d^3$. Thus particles differing only 2-fold in d differ 8-fold in ℓ and, as shown by eq 1, they differ approximately 8-fold in flow displacement velocity as measured by $\mathcal{V}$ or R. With such large differences in $\mathcal{V}$ and R values and consequently in elution times, the particles are readily separated. Because of this high sensitivity of ℓ to d, particles differing by only 10% in d can be separated by Sd/Nl FFF.

The negative aspect of the high sensitivity of ℓ (and thus of $\mathcal{V}$) to d is that for particles spanning a wide d range the differences in $\mathcal{V}$ become unmanageably large, and particles of the largest diameter are eluted from the system much too slowly. Thus, for a 10-fold d range, the ℓ value for the smallest particles is 10^3 times larger than that of the largest particles. Thus, the smallest particle will migrate approximately 1000 times faster than the largest particle and elute 1000 times earlier. However, to maintain reasonable resolution, the smallest particle requires a small ℓ (e.g., $\ell < 100$ μm) and a finite time for elution, usually $\geq$3 min. Hence, the largest particle would elute in $\geq$3000 min, which is far too long for practical analytical purposes.

The programming methods introduced in 1974 (*10*) were intended to offset this excessive range of elution time as follows. Some parameter that controls migration velocity $\mathcal{V}$ is varied during the run such that, following elution of the smaller particles, the $\mathcal{V}$ of the larger particles is forced to increase so that their retention times are decreased. Among the parameters that can be varied to achieve this objective are field strength, flow velocity, and various properties of the carrier fluid, including density. Field strength S is the most important variable used in programmed FFF. Thus in *programmed FFF*, S (to which the primary driving force is proportional) is started at a high level suitable for the separation of the smallest particles. As the run progresses, S is gradually diminished. As S decreases, U decreases in proportion to S and, as shown by eq 2, ℓ then varies as $1/S$. Consequently, for the larger particles, for which ℓ and $\mathcal{V}$ are initially very small, the ℓ value increases, because of the programming, up to the point where the particles acquires a moderate $\mathcal{V}$ and elute in a reasonable time. Thus the problem of an excessive time range associated with a large diameter or molecular weight range in the normal operating mode of FFF can be combated by field-programmed FFF or related programming schemes.

Since the initial development of programmed Sd/Nl FFF (*10*), a number of papers have appeared describing different ways of carrying out programming, including the programming of flow (*13*, *25*), application to thermal FFF (*11*, *19*, *26*), application to flow FFF (*15*, *17*, *18*), and different specific mathematical forms for the programming of field strength (*10–14*, *27*). All of the above cited literature, including all of the theory and experimental implementation, is focused on

the normal operating mode of FFF and is based on the rationale described above. The only exception is a recent paper in which programming of the cyclical-field mode of FFF is discussed (*28*).

Since steric FFF was first developed in the late 1970s (*23*), a considerable literature has evolved on its implementation (*29–31*). However, programming methods have not been utilized for steric FFF. The reasons can be attributed to the vastly different mechanisms of steric FFF and normal FFF.

Steric FFF is generally applied to particles of larger diameter (usually >1 μm) than normal FFF. For these larger particles, diffusion is ordinarily negligible in opposing the primary driving force. Thus these large particles are driven by the primary force directly to the accumulation wall as shown in Figure 1b. Their motion is stopped by essentially "bumping" into the wall, and thus they reach a state of equilibrium in close proximity to the wall. Particles of large size protrude further into the channel than those of small size and are caught up in streamlines of higher velocity (Figure 1b). Therefore the large particles are displaced more rapidly by flow and are eluted earlier than the small particles. Consequently the elution order is inverted relative to that of normal FFF.

Based on the above steric mechanism, the effective particle elevation (essentially the center of gravity elevation) above the accumulation wall is approximately equal to the particle radius a. The migration velocity $\mathcal{V}$ caused by flow is thus approximately proportional to a much as it was found proportional to ℓ for normal FFF. The retention ratio R is given by (*29, 32*)

$$R = 6\gamma a/w \tag{3}$$

which resembles eq 1 with ℓ replaced by γa. The dimensionless steric correction factor γ accounts for hydrodynamic effects. For steric FFF, $\gamma \cong 1$.

Equation 3 shows that R and thus $\mathcal{V}$ increase roughly as particle radius or diameter. Consequently, if a sample contains particles whose maximum and minimum diameters differ 10-fold, the largest particles should migrate 10 times faster than the smallest particles. This 10-fold range in $\mathcal{V}$ and thus in elution times is quite acceptable, in contrast to the unacceptable 1000-fold elution time range associated with a similar diameter range in Sd/Nl FFF. Thus, among other considerations, programming is not generally needed in steric FFF to avoid excessive run times. For example, Koch and Giddings (*29*) achieved the base-line separation of seven different sizes of latex spheres from 2 to 45 μm in diameter (more than a 20-fold size range) in under 4 min.

Still another factor that has discouraged programming in steric FFF is the lack of an effective means of programming. According to the simple model of steric FFF described above, the migration velocity depends only upon the particle size and not on the field strength. Thus, field programming, according to this mechanism, could not possibly be beneficial. Flow programming could be used, but the resolution of the large particles eluting first is less degraded by high flow rates than the small particles eluting last. Consequently, the highest flow rate consistent with small-particle resolution should be used for the beginning of the run, without programming.

Recent work has clarified the mechanism of steric FFF (e.g., see ref 29). It is now clear that particles do not make actual contact with the accumulation wall but are held a small distance away by hydrodynamic lift forces. When sedimentation is used as the primary driving force, as in all the early work in steric FFF (*23, 33–35*), these lift forces further reduce the selectivity, leading to a dependence of $\mathcal{V}$ on d raised to a power of 0.5–0.8 (*22, 30, 32*). Thus, a 10-fold diameter range elutes over a time range of $10^{0.5}$–$10^{0.8}$, or 3.2–6.3. Even a 50-fold d range has a time range of only 7–23. This time range is too narrow to justify programming, particularly since an effective programming mechanism is not apparent.

Another operating mode of FFF is the *hyperlayer mode* (Figure 1c), in which different particle populations are forced into narrow bands (called hyperlayers) located at different elevations above the accumulation wall (*36–38*). A subclass of hyperlayer FFF is *lift hyperlayer FFF*, in which hydrodynamic lift forces drive particles away from the wall and into their respective equilibrium hyperlayers (*39–41*). Lift hyperlayer and steric FFF form a continuum, with lift hyperlayer FFF applicable when the effects of hydrodynamic lift forces dominate pure steric effects. Arbitrarily, the steric mode is considered applicable when $\gamma < 2$, and the lift hyperlayer mode when $\gamma \geq 2$. The lift hyperlayer mode appears to work effectively only when the primary driving force F is weakly dependent on diameter d. Specifically, F should increase with *less than* a third-power dependence on d. Thus, the sedimentation version of lift hyperlayer FFF, sedimentation/hyperlayer FFF, does not appear to be very effective. However, a cross flow force, with a first-power dependence on F on d, yields excellent results (*22, 40, 41*).

In the resulting subtechnique, *flow/hyperlayer FFF* (Fl/Hy FFF), the sensitivity of $\mathcal{V}$ to d is substantially greater than that of sedimentation/steric FFF (*22*). This increased selectivity expands the time range over which different particle diameters elute; a 10-fold d range will generally emerge over a time range of 16–32. This time range, although rather large, does not constitute a serious problem as in Sd/Nl FFF, where the time range is 1000. However, a serious problem does exist in that experimental conditions suitable for large particles cannot in most cases be used for small particles. Large particles (e.g., 20–40 μm), for reasons explained below, require high field strengths and low channel flow rates. Under these conditions, it has been observed in our laboratory (*22*) that small particles (typically <3 μm), as well as certain macromolecules (*15*), become immobilized (probably due to adhesion to the accumulation wall) and cannot be eluted through the channel. Thus it has not been found possible to elute and resolve small particles under conditions favorable to large particles. However, if low fields and/or high channel flow rates are used, the small particles can be eluted and resolved, but then the resolution of large particles fails.

We have found that the above difficulties, characteristic of Fl/Hy FFF, can be removed by programming the field, programming the channel flow velocity, or programming both (i.e., *dual programming*). This finding is unexpected because of the close relationship of lift hyperlayer FFF to steric FFF, which, it appears, cannot be effectively programmed. The fundamental basis for this observation, as it is now understood, is as follows.

A major factor affecting the coefficient γ in eq 3, as pointed out above, is the exertion of hydrodynamic lift forces on particles driven through narrow conduits by flow (*42–48*). These rather complicated forces tend to drive particles away from walls. If the primary driving force is relatively small, the particle may be driven several diameters from the wall before equilibrium is established between the primary driving force and the opposing lift forces. A particle so far from the wall will be caught up in relatively fast streamlines and will migrate more rapidly (and thus have a higher R) than its counterpart undergoing steric FFF migration close to the wall. Equation 3 shows that R increases in proportion to γ for constant a and w. When $\gamma \geq 2$, the particle is removed one radius or more above the position at which it makes contact with the wall. Under these conditions, which correspond to lift hyperlayer FFF, particles of a given diameter form a thin equilibrium hyperlayer elevated above the accumulation wall of the FFF channel. The elevation of the hyperlayer, and thus

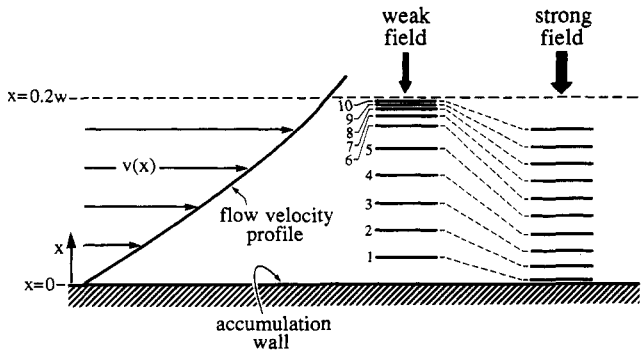

Figure 2. Illustration of hyperlayer positions for a series of 10 particles of systematically increasing diameter. These positions, shown by the horizontal bars, are crowded closely together for the larger numbered (and thus larger diameter) particles under weak field conditions. These closely crowded hyperlayers, when displaced by the flow velocity profile shown, migrate at almost equal velocities and are poorly resolved. Under strong field conditions, the spacing between large-particle hyperlayers increases and the differential migration and thus the resolution are improved.

the value of γ, is influenced by both the field strength and the flow rate. If the field strength is increased, the particle is driven closer to the wall and γ decreases. If the flow rate is increased, the hydrodynamic lift forces gain in magnitude and the particle is driven further from the wall, leading to an increase in γ (*45–48*). Thus the particle equilibrium elevation can be controlled by changes in both field strength and flow rate. Such changes in elevation must be realized in the course of a run in order to elute small particles and still resolve large particles in the same run.

The high selectivity of Fl/Hy FFF is related to the fact that lift forces increase rapidly with particle size, depending on the third or fourth power of d (*48*). If the opposing driving force has less than a third-power dependence on d, as specified above for effective lift hyperlayer FFF, then the resulting hyperlayer elevation, driven by the lift forces, will tend to increase rapidly with d. However, when the hyperlayer elevation reaches ~20% of the channel thickness w, the lift forces, for complicated hydrodynamic reasons, approach zero (*45–47*). Thus, if particles of a given d are driven to an elevation close to $0.2w$, then particles twice as large, instead of being driven to a much higher elevation where they would be separated from the original particles, are also confined by the effective ceiling near $0.2w$. Therefore, both particle sizes, although differing 2-fold in diameter, are driven to approximately the same elevation and thus migrate at approximately the same velocity. Consequently, there is very little resolution between the particles in this size range.

The above problem can be overcome by increasing the field strength and/or decreasing the flow velocity. With these changes, the smaller particles (in the large particle set under consideration) will be driven well below the ceiling elevation of $0.2w$ and will thus separate from the larger particles approaching the $0.2w$ elevation level. Thus selectivity is restored. By varying the field strength and the flow rate up and down, it is possible to maximize the selectivity and thus the resolution for any given pair of particles.

Figure 2 illustrates the mechanism by which the resolution of large particles is improved by an increase in field strength. (A decrease in flow rate has the same effect). This figure shows the approximate ceiling elevation for particle hyperlayers at $x = 0.2w$. (The ceiling at $0.2w$ is an idealization; the actual ceiling will vary slightly with a number of parameters, including d.) The hyperlayer position of 10 different particles for which the diameter increases systematically from 1 to 10 (e.g., in the range 2–50 μm) are shown by the numbered horizontal bars. The bars at the left show these positions under weak field conditions. With a weak field strength, the smaller particles are spaced rather evenly while the positions of the larger particles become compressed against the "ceiling". Each hyperlayer is displaced downstream at the approximate velocity $v(x)$ of the flow vector found at the hyperlayer (particle center of gravity) elevation. Because the positions of the larger particles are crowded closely together, $v(x)$ will differ little among them. Thus, their migration velocities will be approximately equal and the resolution of the particles will be poor. The smaller particles, having a larger relative gap between hyperlayer positions and a larger relative difference in $v(x)$ values, will be more fully resolved. However, with an increase in field strength, all of the hyperlayer positions will be displaced downward from the ceiling, as shown by the right-hand set of horizontal bars, and larger and more even intervals will appear between the large-particle hyperlayers. This will improve the resolution realized between the large particles.

Small particles (e.g., <3 μm) are subject to different forces and have different requirements. Because of the strong dependence of lift forces on d, the smaller particles are subject to quite weak lift forces. The primary driving force is also smaller but it does not decrease as rapidly with d because the dependence is less than third power. Thus the primary driving force gains dominance over the lift forces as the diameter decreases, providing the conditions remain constant. Consequently, small particles are driven very close to the wall and those below a certain threshold diameter are observed to be captured. However, it has been found, particularly when cross flow is used as the driving force, that the immobilization of particles at the wall is reversible (see later). Thus, if conditions are shifted such that the primary driving force is no longer dominant, the particles can once again be mobilized and eventually eluted and resolved. In order to induce the mobilization of immobilized particles, one can either reduce the primary driving force by reducing the field strength or increase the lift forces by increasing the flow rate. For maximum effectiveness, both can be done simultaneously.

Because large particles and small particles have such different requirements for their successful separation, it would appear that these two populations could not be resolved in a single run. However, we find that both populations can be separated at high resolution levels by using field programming, flow programming, or dual programming, a combination of the two. The procedure works as follows.

Following the injection of sample particles, the run is started with conditions adjusted for the effective resolution of the largest particles. This means specifically that the initial field strength is sufficiently high or the initial flow rate is sufficiently low that all but the very largest particles of interest are driven away from the ceiling position at $0.2w$. Under these conditions, the large particles migrate rapidly down the channel, undergoing separation as they proceed. Meanwhile, the particles below the threshold diameter are effectively immobilized by the dominance of the primary driving force over the lift forces. Consequently, these particles undergo little or no migration and separation in this initial stage of the run.

The field strength is now programmed downward or the flow velocity upward, or both. This should not be done too abruptly or it will hinder the high resolution of the large particles. However, once large-particle separation is assured, then the field strength and/or flow rate can be sufficiently altered such that the medium-sized particles migrate and separate. As the programming continues, the smallest particles of interest are mobilized under conditions that are now suitable for their resolution. Consequently, the whole particle size range can be eluted and separated in a single run.

We note that the mechanism responsible for the immobilization of components is not fully understood. Reversible

immobilization has been observed for both particles and macromolecules (such as proteins) when cross flow is used as a driving force (*15*). Whatever the mechanism, the above programming scheme should expand the useful range of application of lift hyperlayer FFF. Even if the smaller particles are not technically and fully immobilized, but only reduced in migration velocity because of their initial position close to the wall, programming will speed up their elution and thus allow the more rapid completion of the FFF run.

We observe that programming in lift hyperlayer FFF bears a superficial resemblance to programming in normal-mode FFF, both bearing a still more distant relationship to programmed chromatography. However, there are such major differences between lift hyperlayer and normal FFF in matters such as elution order, separable particle size range, and basic programming mechanism that success in one area does not assure workability in the other.

Programmed lift hyperlayer FFF and programmed normal FFF are designed to solve a different set of problems, one being the immobilization of smaller particles in the lift hyperlayer case. In normal FFF, smaller particles elute first instead of last and are least likely to immobilize. Also, in normal FFF, the resolution of the late-eluting larger diameter particles is very high; the main purpose of programming is to hasten their elution. In lift hyperlayer FFF, large particles elute but programming is needed to resolve them under conditions also suitable for resolving small particles.

In lift hyperlayer FFF, where the small particles elute last, a secondary goal of programming is to hasten the elution of the small particles, but the primary goal remains that of providing conditions that circumvent small-particle immobilization and large-particle resolution loss. The time question is a less critical matter with lift hyperlayer FFF both because of the intrinsically higher speed of lift hyperlayer FFF compared to normal FFF and because of the fact noted earlier that the elution time range for a given span of diameters is not nearly as large in lift hyperlayer FFF as it is for Sd/Nl FFF.

We note further that lift hyperlayer FFF is an outgrowth of steric FFF, where programming has not been found practical. Lift hyperlayer FFF differs from steric FFF by virtue of the important influence of lift forces, without which programming would be of no consequence. The smaller particles separated by normal FFF are influenced only slightly by lift forces, which are thus not a factor in the programming of normal FFF.

Finally, along with the fact that the elution order is opposite in lift hyperlayer FFF compared to normal FFF, the size ranges to which these techniques are applicable are quite different. Normal FFF is generally applicable up to 1 μm in diameter whereas lift hyperlayer FFF, while capable of separating particles below 1 μm, is mainly a large-particle separation technique effective up to 50 μm in diameter or higher.

THEORY

Because of the mathematical complexity of hydrodynamic lift forces and unresolved questions about their origin (*48*), retention in steric and lift hyperlayer FFF cannot be calculated on the basis of simple mathematical expressions as found possible for normal FFF. While the retention ratio R is given quantitatively by eq 3, the uncertainties in retention are passed on to the steric correction factor γ, which is found empirically to depend upon particle diameter, field strength, and channel flow rate (*32*).

At present, the best means for characterizing retention originates in the empirical observation that a plot of log t_r (where t_r is the retention time) versus log d yields a straight line over a finite range of particle diameters for both steric and hyperlayer FFF (*30, 40*). The mathematical expression for this linear relationship is

$$\log t_r = -S_d \log d + \log t_{r1} \tag{4}$$

where S_d is the diameter-based selectivity defined by (*49*)

$$S_d = \left|\frac{d \log t_r}{d \log d}\right| \tag{5}$$

and where t_{r1} is a constant equal to the retention time of a particle of unit diameter.

It is useful to express eq 4 in terms of the dimensionless time t_r/t^0 where t^0 is the channel void time, the retention time of a nonretained species. Equation 4 thus becomes

$$\log (t_r/t^0) = -S_d \log d + \log (t_{r1}/t^0) \tag{6}$$

The constants S_d and t_{r1} are obtained from experimental retention time plots based on either eq 4 or eq 6.

When eq 6 is converted to a nonlogarithmic form, we have

$$t_r/t^0 = (t_{r1}/t^0)d^{-S_d} \tag{7}$$

which shows that t_r is inversely dependent upon d to the S_d power. The ratio t_r/t^0 is equal to the reciprocal of the retention ratio (i.e., $1/R$), making it possible to express the latter as

$$R = (t^0/t_{r1})d^{S_d} \tag{8}$$

When eq 8 is equated to eq 3, the steric correction factor γ emerges as

$$\gamma = (w/3)(t^0/t_{r1})d^{S_d-1} \tag{9}$$

which shows how γ depends upon the empirical calibration constants S_d and t_{r1}. Since S_d is generally greater than unity for lift hyperlayer FFF, γ is seen to increase with diameter d. The dependence of γ on cross and channel flow rates will emerge from eq 9 mainly through the dependence of γ on t_{r1}, although the quantitative form of the dependence of t_{r1} upon both flow rates has not been established.

In normal FFF, where retention (as well as band broadening) is subject to fewer uncertainties, the quantitative expressions applicable to nonprogrammed FFF can be extended to various programmed forms of FFF. Because of this mathematical tractability, retention and resolution can be calculated when the programs assume different mathematical forms (*10, 50, 51*). For example, it has been shown that when the field strength decays according to a power function (see later), the resolving power for a given fractional diameter difference (i.e., the fractionating power) is constant over a wide range of particle sizes (*27*). Unfortunately, such definite theoretical conclusions cannot be drawn for lift hyperlayer FFF, for which the efficacy of various programs can only be established by empirical examination.

For field programming, the field strength S is generally varied with time, as dictated by some applied mathematical function. There are virtually an infinite number of specific programming functions that can be utilized, including those falling in parabolic, linear, exponential, stepped, and power categories, and their combinations. The two used in this work are linear and power programming functions.

A linear decay in the field strength is described by (*51*)

$$S(t) = S_0[(t_1 + t_p - t)/t_p] \tag{10}$$

over the time interval $(t_1 + t_p \geq t \geq t_1)$, where $S(t)$ is the field strength at time t, S_0 is the initial field strength, t_1 is the predecay time (the time between the start of the run and the start of the decay), and t_p is the linear program time. For flow FFF, the field strength is expressed as the cross flow rate $\dot{V}_c$. Therefore, eq 10 can be rewritten as follows in terms of $\dot{V}_c$ and the initial cross flow rate $\dot{V}_{c0}$:

$$\dot{V}_c(t) = \dot{V}_{c0}[(t_1 + t_p - t)/t_p] \quad (11)$$

The power program for a decaying field is described by (27)

$$S(t) = S_0[(t_1 - t_a)/(t - t_a)]^p \quad (12)$$

where t_a is an arbitrary time constant and p is the power parameter. The requirements for these parameters are $t \geq t_1 > t_a$, $t_1 \geq 0$, and $p > 0$. In the normal mode, the optimum condition (corresponding to uniform resolution) occurs when p is set equal to a particular value determined by the field type (e.g., 8 for sedimentation and 2 for cross flow) and when the relationship $t_a = -pt_1$ (with $t_1 \neq 0$) is fulfilled (27). For flow FFF, eq 12 can be expressed in terms of the cross flow rate

$$\dot{V}_c(t) = \dot{V}_{c0}[(t_1 - t_a)/(t - t_a)]^p \quad (13)$$

For a program of increasing channel flow rate $\dot{V}$ (as opposed to decreasing cross flow rate $\dot{V}_c$), the power program function becomes

$$\dot{V}(t) = \dot{V}_0[(t_2 - t_b)/(t - t_b)]^q \quad (14)$$

where $\dot{V}(t)$ is the volumetric flow rate at time t, $\dot{V}_0$ is the initial flow rate, t_b is an arbitrary time constant, t_2 is the time the channel flow rate is held constant before increasing, and q is the power of the function. The conditions for these parameters are $t \geq t_2 > t_b$, $t_2 \geq 0$, and $q < 0$. For reasons similar to those for the programmed field case, the parameters are normally constrained by $t_b = qt_2$ and $t_2 \neq 0$ (52).

The volume V of the carrier that has flowed longitudinally through the channel from the start of the run can be calculated by integrating eq 14 with respect to time:

$$V = \int_0^t \dot{V}\, dt = \dot{V}_0 t_2 + \dot{V}_0 \int_{t_2}^{t} \left(\frac{t_2 - t_b}{t - t_b}\right)^q dt \quad (15)$$

where the contribution due to the constant channel flow rate period is equal to $\dot{V}_0 t_2$. Carrying out the integration and rearranging, we get

$$V = \dot{V}_0 t_2 + \frac{\dot{V}_0}{(1 - q)}\left[\left(\frac{t_2 - t_b}{t - t_b}\right)^{q-1} - 1\right](t_2 - t_b) \quad (16)$$

An equivalent expression can be derived for the total cross flow volume. The agreement between the measured and calculated volumes (hence, flow rates) in a programmed run can thus be determined. These volumes are used to monitor the channel flow rates, which are not measured directly.

A similar integration procedure can be performed for any other program type to obtain the analogous equations for total channel and cross flow volumes.

EXPERIMENTAL SECTION

Apparatus. A schematic diagram of the flow FFF system used in this study is shown in Figure 3. A pneumatic-actuated injection valve, Model 7010, from Rheodyne (Cotati, CA) was used to introduce a 20-μL volume of sample to the system. The channel flow pump (Model 410, Kontron Electrolab, London, England) provided the flow along the longitudinal axis. The cross flow field was a second flow of carrier driven across the system by a laboratory-built syringe pump. Both pumps were calibrated at the onset of this work. The UV detector (Spectroflow 757, Applied Biosystems, Ramsey, NJ) was set at 254 nm with an absorbance range of 0.02 or 0.05 full scale.

The flow FFF channel consists of two Plexiglass blocks that are clamped together over a Mylar spacer from which the channel volume has been cut and a semipermeable membrane that serves as the accumulation wall. Porous frit panels are set into the Plexiglass blocks to allow the cross flow to be driven across the channel system (top frit, spacer, membrane, and bottom frit). The channel has dimensions of 27.2-cm tip-to-tip length, 2-cm breadth, and ≅0.0254-cm thickness. A 30 000 molecular weight cutoff membrane (Amicon YM30, Amicon Corp., Danvers, MA) is used as the accumulation wall in these experiments. The resulting channel is oriented vertically to avoid gravitational field effects.

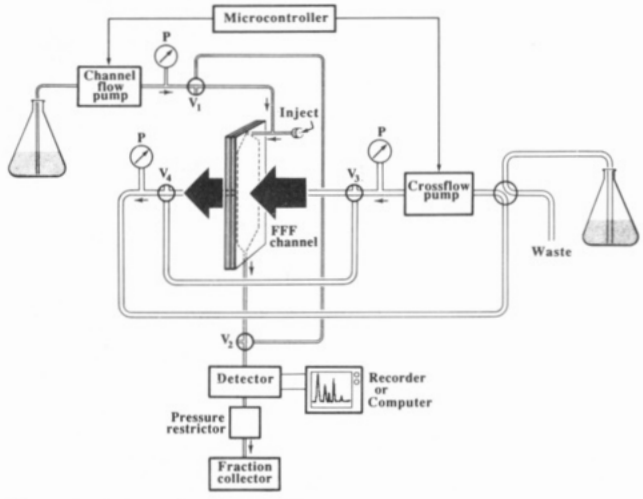

Figure 3. Schematic diagram of computer-controlled flow FFF system. The valves are denoted by V_1–V_4 and the pressure gauges by P.

Microcomputer-Based Program Controller. A microcomputer-based flow controller, designed and built in conjunction with the departmental electronics shop, was interfaced to the channel flow and cross flow pumps. The microcomputer utilizes an Intel 8052 microcontroller. Its primary purpose is to regulate the cross and channel flow rates according to the information that is input prior to a programmed run. Queries are made concerning the number of flow rates to be programmed, the type of program (e.g., linear, power, exponential, etc.), and the numerical values of the appropriate programming parameters. The depression of the RUN button initiates the experimental process. Usually, the time-dependent process is preceded by a period of time in which the field strength and channel flow rate are held constant at chosen initial values. When the programmed variation commences, the controller updates the flow rate of each pump at 1-s intervals.

The fidelity of the experimental channel flow rates to the calculated flow rates during a programmed run was verified by measuring the total volume of carrier that eluted from the system at various time intervals and comparing it to the theoretical volume. Equation 16 was used in these volume calculations. The cross flow rate was not verified in this manner. During programmed operation, the syringe pump that drives the cross flow is connected to the FFF channel in a looped configuration (Figure 3). The flow rate of the cross flow stream entering the channel should equal that being withdrawn. One improvement to the plumbing scheme would be the incorporation of a flowmeter into the cross flow loop. This would enable a more direct confirmation of the cross flow rate variation with respect to time. The flow rate(s) is(are) continuously varied until it(they) reach(es) a preset hold value. The experiment is over when the STOP button is depressed.

Reagents and Samples. The carrier liquid was distilled deionized water to which had been added 0.1% (w/w) of FL-70 surfactant (Fisher Scientific, Fairlawn, NJ) and 0.02% (w/w) sodium azide. The polystyrene latex standards used have nominal diameters of 47.9, 40.1, 29.12, 19.58, 15.00, 9.87, 7.04, 5.002, 3.009, 2.062, and 1.05 μm. These standards will be referred to as 48-, 40-, 29-, 20-, 15-, 10-, 7-, 5-, 3-, 2-, and 1-μm particles, respectively. Mixtures were made from the standards as supplied, relative amounts being adjusted to provide acceptable peak heights. The standards are from Duke Scientific Corp. (Palo Alto, CA) with the exception of the 1-μm latex, which is from Polysciences, Inc. (Warrington, PA).

RESULTS AND DISCUSSION

Dual programming of the field strength (cross flow rate $\dot{V}_c$) and channel flow rate $\dot{V}$ is complicated in flow FFF because it requires the accurate and independent control of the flow rates of two streams passing through a common chamber—the FFF channel. The agreement between the calculated and

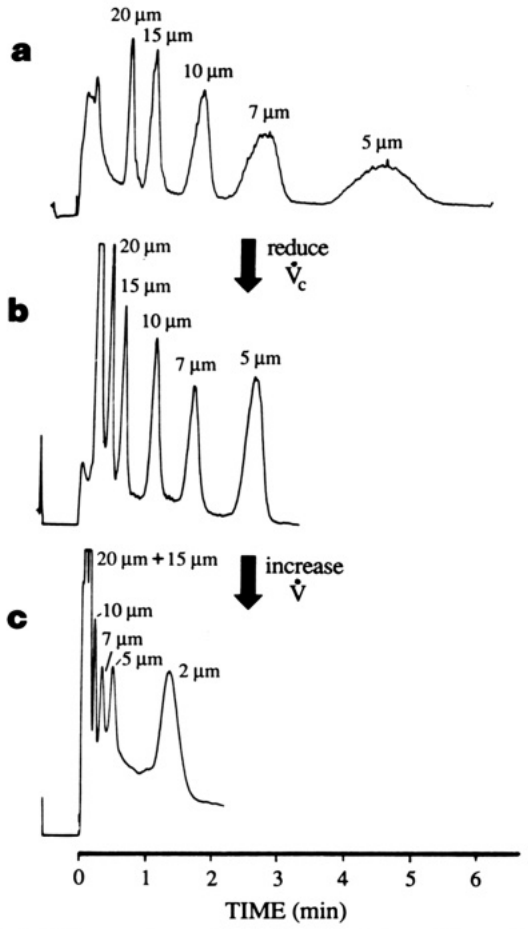

Figure 4. Influence of cross flow rate $\dot{V}_c$ and channel flow rate $\dot{V}$ on the separation of polystyrene latex beads: (a) $\dot{V}_c$ = 3.33 mL/min, $\dot{V}$ = 3.93 mL/min; (b) $\dot{V}_c$ = 0.98 mL/min, $\dot{V}$ = 3.91 mL/min; (c) $\dot{V}_c$ = 0.98 mL/min, $\dot{V}$ = 8.69 mL/min.

measured channel flow rates was verified by measuring the cumulative volume of carrier passed through the channel at various time intervals. The volumes were calculated from eq 16 or equations that were derived in a similar manner. The agreement between the calculated and measured volumes was within 4%.

The effect of changes in the cross and channel flow rates on particle fractionation, discussed conceptually earlier in this paper, are illustrated in Figure 4. This figure shows fractograms obtained under different flow conditions with the injection of a sample mixture of 20-, 15-, 10-, 7-, 5-, and 2-μm latex beads. In Figure 4a, with $\dot{V}_c$ and $\dot{V}$ equal to 3.33 and 3.93 mL/min, respectively, the larger particles (down to 5 μM) are well resolved in slightly over 5 min, but the 2-μm particles fail to appear because of the immobilization effects discussed earlier. When the cross flow is reduced 3.4-fold to 0.98 mL/min (with the channel flow rate remaining essentially constant at 3.91 mL/min), the peaks are still well resolved but elute considerably earlier, as illustrated by Figure 4b. The change in the time of elution can be explained in terms of the expansion of the particle hyperlayers upon going from a strong field to a weak field, as illustrated in Figure 2. The effect is shown quantitatively in Figure 5, where the actual hyperlayer positions are plotted for the different experimental cases shown in Figure 4. The specific positions are calculated from the equation $\mathcal{V} = v(x)$, where $\mathcal{V}$ is obtained from the measured retention times and where the hyperlayer elevations (x) are calculated by assuming a parabolic flow profile for $v(x)$.

As discussed earlier, much the same effect is observed upon decreasing $\dot{V}_c$ is found upon increasing the channel flow rate $\dot{V}$, which enhances the hydrodynamic lift effects. The ex-

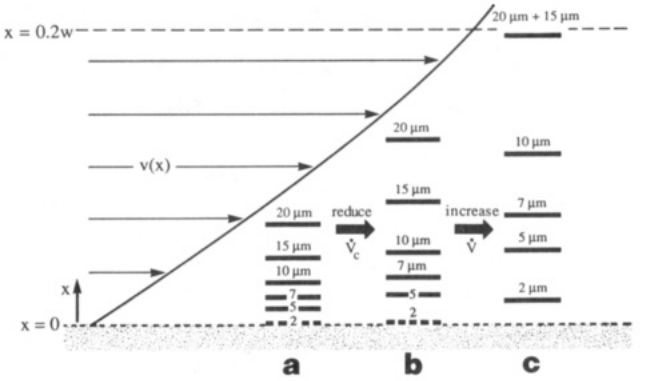

Figure 5. Calculated equilibrium hyperlayer positions for the particles separated in Figure 4.

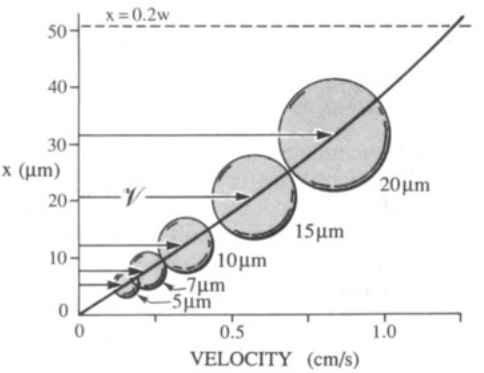

Figure 6. Diagram showing the relative scaling of particle diameters and hyperlayer positions for the fractogram shown in Figure 4b. The velocity $\mathcal{V}$ of migration of each of the particles is shown by the abscissa (velocity) scale.

perimental effects of a 2.2-fold increase in $\dot{V}$ (i.e., $\dot{V}$ = 8.69 mL/min with $\dot{V}_c$ constant) are shown by the comparison of parts c to b in Figure 4. The retention times associated with the larger value of $\dot{V}$ are decreased further and the large particle peaks are partially or totally fused together because of the hyperlayer compression effects near $x = 0.2w$. The latter is illustrated on the right-hand side of Figure 5. However, with the increased influence of lift forces relative to the primary driving force induced by cross flow, the 2-μm particle makes its appearance well resolved from the preceding 5-μm peak.

The actual scaling of distances and velocities within the FFF channel for a typical Fl/Hy FFF run (shown by Figure 4b) is conveyed by Figure 6. Here the particle diameters are shown in relationship to the hyperlayer elevations, with each particle properly positioned on the parabolic flow displacement curve. Note that each sphere is well removed from the accumulation wall (at $x = 0$) as a consequence of the hydrodynamic lift forces.

The series of experimental fractograms in Figure 4 illustrates the difficulty of finding a single set of conditions suitable for the resolution of both large and small particles, even over a limited 10-fold d range. It is this difficulty that programming is intended to resolve.

The effect of programming the field strength and/or the channel flow rate is demonstrated in Figure 7. Variations in the cross and channel flow rates as each run progresses are depicted above the fractograms as solid and dashed lines, respectively. The reference fractogram shown in Figure 7a was obtained with both flow rates constant, $\dot{V}_c$ = 2.18 and $\dot{V}$ = 3.00 mL/min. The peaks correspond to polystyrene latex standards with diameters from 48 to 7 μm, as identified in the figure. Conspicuously absent from this fractogram are peaks for the elution of 5- and 2-μm beads, which were also present in the injected sample mixture. The absence of these

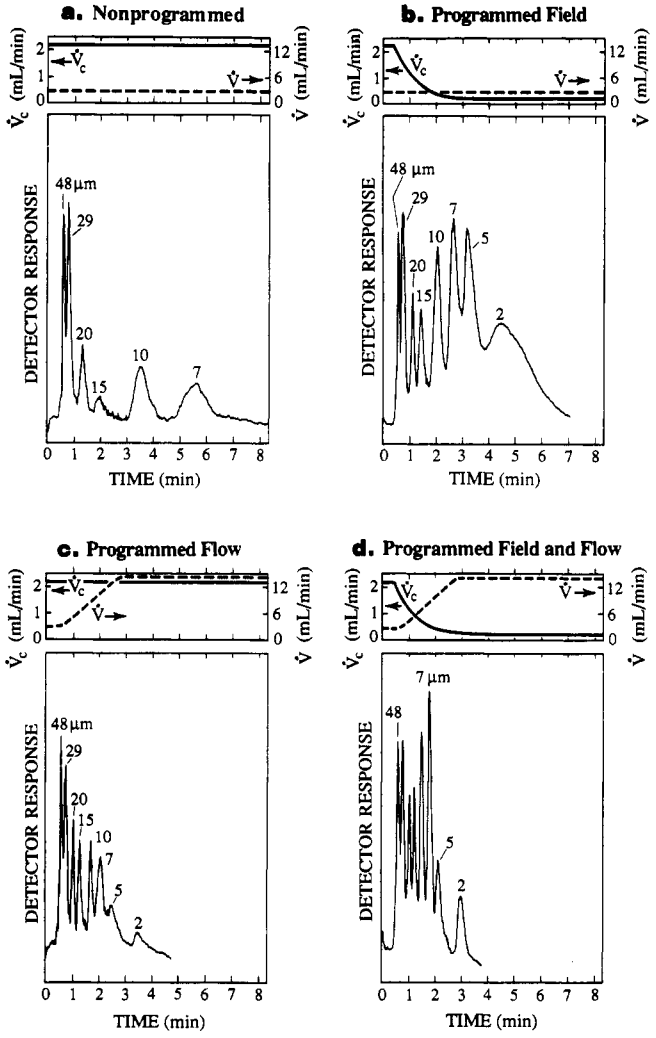

Figure 7. Effect of field and flow programming on the separation of polystyrene latex standards of diameters 48, 29, 20, 15, 10, 7, 5, and 2 μm. Variations in the cross and channel flow rates are represented by solid and dashed lines, respectively, above each fractogram. (a) Constant conditions: $\dot{V}$ = 3.00 mL/min, $\dot{V}_c$ = 2.18 mL/min. (b) Programmed field: $\dot{V}$ = 3.00 mL/min, $\dot{V}_c$ = 2.18 mL/min decaying to 0.25 mL/min, p = 3, t_1 = 30 s, t_a = −90 s. (c) Programmed flow: $\dot{V}$ = 3.00 mL/min increasing to 14.00 mL/min, q = −1.5, t_2 = 30 s, t_b = −45 s, $\dot{V}_c$ = 2.18 mL/min. (d) Programmed field and flow: conditions are the same as 7b for $\dot{V}_c$ and 7c for $\dot{V}$.

two peaks is attributed to immobilization of the particles by the membrane.

Figure 7b illustrates the results of a power-programmed decay of the field strength. The initial conditions are identical to those used in the isocratic separation, that is $\dot{V}$ = 3.00 and $\dot{V}_c$ = 2.18 mL/min. After an initial stop flow time of 50 s, the channel flow is resumed and the field strength is held constant for a time interval (predecay time) t_1 of 30 s. The variation in the cross flow rate is dictated by eq 13. The t_a value, calculated on the basis of the condition $t_a = -pt_1$, where p = 3, is equal to −90 s. The time (156.9 s) at which the field reaches the hold value of 0.25 mL/min is calculated by the microcomputer, based on the parameters entered.

In Figure 7b, as a consequence of the field programming, both the 5- and 2-μm particle standards elute as distinct peaks. The elution of these two components in a field-programmed run (in which the starting conditions are inconsistent with their migration) illustrates that their immobilization by the membrane under nonprogrammed conditions (as shown in Figure 7a) is a reversible process. The total analysis time is still only 6 min (plus an additional 50-s stop flow time) despite the broader particle diameter range.

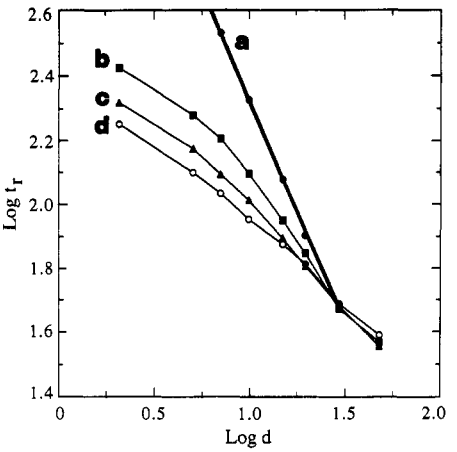

Figure 8. Calibration plots derived from the fractograms of Figure 7: (a) constant conditions, (b) programmed field, (c) programmed flow, and (d) dual-programmed field and flow.

Figure 7c illustrates the use of channel flow programming. In this case, the cross flow rate is held constant at the previous starting level of 2.18 mL/min and the channel flow rate is increased from 3.00 to 14.0 mL/min with q = −1.5, t_2 = 30 s, and t_b = −45 s. Once again, 2- and 5-μm microspheres are mobilized by the programming. The separation of 2–48-μm particles is now completed within 4 min.

Finally, an example of the dual programming of the two flow rates is given in Figure 7d. The cross and channel flow rates are simultaneously decreased and increased, respectively, using the same program parameters specified for the fractograms shown in parts b and c of Figure 7. The analysis time is further shortened to 3.5 min. The widths of the peaks shown in Figure 7d are approximately constant, with the exception of the 2-μm peak, which is broader. The fractogram displays a nearly uniform fractionating power, a desirable feature in particle fractionation (27).

Parts a–d of Figure 7 show no observable differences in retention times for components eluting within the first 50 s. This is due to the constant conditions employed in the constant channel flow rate time of 30 s for all the programmed cases. Differences in peak areas in this series of fractograms are a result of inadequate stirring of the particle suspension prior to loading the microsyringe for injection.

We noted earlier that under nonprogrammed conditions, a plot of log t_r versus log d normally yields a linear segment, convenient for calibration (see eq 4). Such log–log plots corresponding to the fractograms of Figure 7 are presented in Figure 8. The plot for the nonprogrammed run, curve a, yields a nearly straight line segment (with a negative slope of 1.37) for d = 7–29 μm, with d = 48 μm being considerably off-line. The plots of the programmed runs show a reduction in slope S_d (equal to selectivity), especially as the particle diameter decreases. This decrease in selectivity is related to the hastened elution of the small-diameter particles. The largest deviation from the nonprogrammed plot occurs for the case of dual programming of the field and channel flow rate (Figure 8d). However, the line for dual programming is close to linear, with a negative slope S_d = 0.49.

Figure 9 demonstrates that different fractograms result when unlike (in this case linear and power) programmed cross flows are employed. In both cases, the channel flow rate is held constant at 4.00 mL/min and the cross flow rate is decreased from 4.00 to 0.25 mL/min. The program parameters for the linear field decay are t_1 = 60 s and t_p = 389.3 s and for the power-programmed field decay p = 3, t_1 = 60 s, and t_a = −180 s. The values for t_a and t_p were selected such that the hold time was reached at the same point (425 s) in both programs. Examination of the curves (shown above the

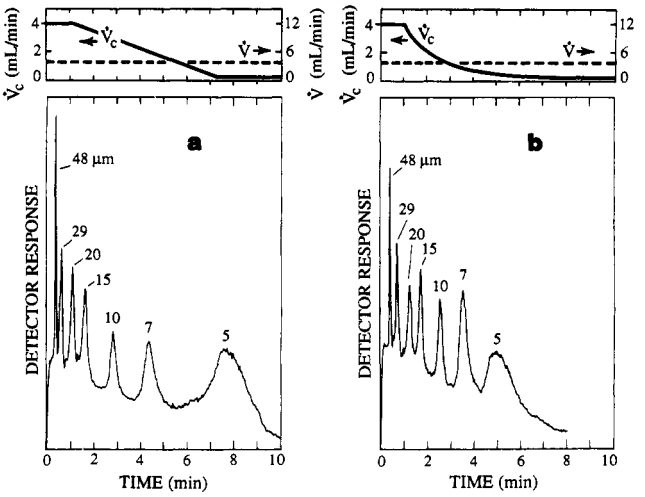

Figure 9. Comparison of linear- and power-programmed field decay experiments. For both, $\dot{V}$ = 4.00 mL/min and $\dot{V}_c$ = 4.00 mL/min decaying to 0.25 mL/min. (a) Linear field decay: t_1 = 60 s, t_p = 389.3 s. (b) Power field decay: p = 3, t_1 = 60 s, t_a = −180 s.

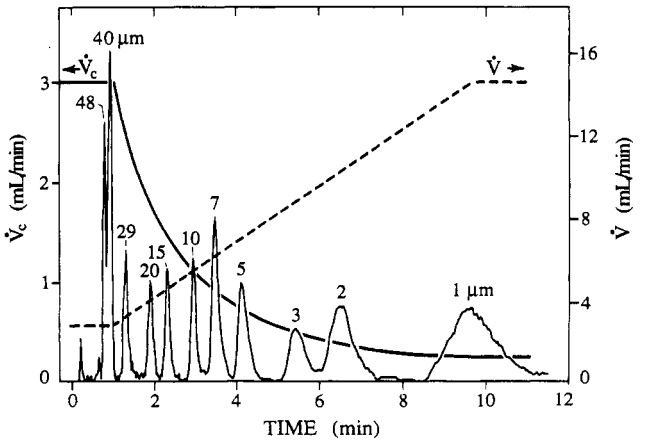

Figure 10. Separation of polystyrene latex standards using dual programming of the cross and channel flow rates. The 11 particle diameters are as shown. The conditions for channel flow are $\dot{V}$ = 3.00 mL/min increasing to 14.5 mL/min, q = −1, t_2 = 60 s, and t_b = −60 s. For cross flow, $\dot{V}_c$ = 3.00 mL/min decaying to 0.25 mL/min, p = 2, t_1 = 60 s, and t_a = −120 s.

fractograms) representing the progression of the cross flow rate for these two cases reveals a marked dissimilarity, explaining why two quite different fractograms are obtained. Since the decay of the power program is initially faster than that of the linear program, the analysis time is significantly shorter for the former. A readjustment of parameters would likely establish better concordance between the two. Further work is needed to compare the two cases under conditions that are optimum for each.

The benefit of dual programming is more fully demonstrated by the fractogram of Figure 10, which was obtained under favorable conditions established by trial and error. The separation of 11 sizes (48, 40, 29, 20, 15, 10, 7, 5, 3, 2, and 1 μm) of polystyrene latex microspheres was accomplished within 11 min under the selected conditions ($\dot{V}_0$ and $\dot{V}_{c0}$ both 3.00 mL/min; final $\dot{V}$ and $\dot{V}_c$ equal 14.5 and 0.25 mL/min, respectively; q = −1, t_2 = 60 s, t_b = −60 s, p = 2, t_1 = 60 s, and t_a = −120 s). All the peaks with the exception of the first two (48 and 40 μm) are base-line resolved. The solid and dashed lines superimposed on the fractogram represent the progression of the cross and channel flow rates, respectively, with respect to time. (This fractogram has been base-line corrected for some drift in the detector signal that resulted from changes in the flow rates.)

The fractionation of particles from 1 to 48 μm demonstrates the broad range in particle diameter that can be separated in a single dual-programmed FFF run under favorable conditions. This 48-fold range considerably exceeds the effective range of the nonprogrammed runs of Figure 4, which are less than 10-fold. It is likely that the dual-programmed range could be further extended by changing the initial and final cross and channel flow rates and other programming parameters. Further investigation is clearly needed in order to optimize the performance of this system.

Work is also needed to ensure that quantitative particle size distribution data can be acquired using these programming methods. When $\dot{V}$ is programmed, two new effects must be accounted for. First, the variable flow through the detector tends to induce base-line drift. If this drift cannot be eliminated, it can be subtracted out, based on a blank run. Second, for a concentration-dependent detector, the flux of particles through the detector at any given time t (corresponding to a specific particle diameter d) is proportional to the product of $\dot{V}(t)$ and the observed signal. Thus, the signal must be corrected for the programmed variations in $\dot{V}$ based on this proportionality. Once this is done, the base-line drift compensated or eliminated, and a calibration curve established (e.g., Figure 8), quantitation should be as straightforward as it is with other FFF techniques.

CONCLUSIONS

Although lift hyperlayer FFF generally, and flow/hyperlayer FFF in particular, differ from normal-mode FFF in mechanism, particle size range, elution order, and intrinsic speed, programming strategies are effective for both. In particular, field and flow programming, used individually or in combination, can enhance separative capabilities. However, in view of the above differences, the basis and the goals of programming are different in the two cases. In lift hyperlayer FFF, programming appears to be essential to expand the applicable size range, whereas in normal-mode FFF, programming is more of a convenience to reduce analysis time for samples having a wide particle size range.

ACKNOWLEDGMENT

We gratefully acknowledge P. Stephen Williams, Marcus N. Myers, and Dale Heisler for their invaluable assistance.

GLOSSARY

a	particle radius
d	particle diameter
D	diffusion coefficient
F	primary driving force
ℓ	mean particle elevation above accumulation wall
M	molecular weight
p	power parameter for power programming of field strength
q	power parameter for power programming of channel flow rate
R	retention ratio
S	field strength
S_d	diameter-based selectivity
$S(t)$	field strength at time t
S_0	initial field strength
t_a, t_b	arbitrary time constants for power programs
t_p	linear program time
t_r	retention time
t_{r1}	retention time of particle of unit diameter
t^0	channel void time
t_1	predecay time
t_2	constant channel flowrate time
U	velocity of transverse displacement toward accumulation wall
$v(x)$	velocity of flow vector
$\langle v \rangle$	mean fluid velocity
$\mathcal{V}$	particle migration velocity

V	volume of carrier passed through the channel
$\dot{V}$	channel flow rate
$\dot{V}_c$	cross flow rate
$\dot{V}_{c0}$	initial cross flow rate
$\dot{V}_0$	initial channel flow rate
w	channel thickness
x	distance above accumulation wall

GREEK

γ	dimensionless steric correction factor

REFERENCES

(1) Giddings, J. C. *Sep. Sci.* **1966**, *1*, 123–125
(2) Giddings, J. C. *Anal. Chem.* **1981**, *53*, 1170A–1175A.
(3) Giddings, J. C. *Sep. Sci. Technol.* **1984**, *19*, 831–847.
(4) Beckett, R. *Environ. Technol. Lett.* **1987**, *8*, 339–354.
(5) Kirkland, J. J.; McCormick, R. M. *Chromatographia* **1987**, *24*, 58–76.
(6) Martin, M. In *Particle Size Analysis 1985*; Lloyd, D. J., Ed.; Wiley: New York, 1987; pp 65–85.
(7) Caldwell, K. D. *Anal. Chem.* **1988**, *60*, 959A–971A.
(8) Giddings, J. C. *Chem. Eng. News* **1988**, *66* (Oct 10), 34–45.
(9) Janca, J. *Field-Flow Fractionation: Analysis of Macromolecules and Particles*; Marcel Dekker: New York, 1988.
(10) Yang, F. J. F.; Myers, M. N.; Giddings, J. C. *Anal. Chem.* **1974**, *46*, 1924–1930.
(11) Giddings, J. C.; Smith, L. K.; Myers, M. N. *Anal. Chem.* **1976**, *48*, 1587–1592.
(12) Yang, F. J.; Myers, M. N.; Giddings, J. C. *J. Colloid Interface Sci.* **1977**, *60*, 574–577.
(13) Giddings, J. C.; Caldwell, K. D.; Moellmer, J. F.; Dickinson, T. H.; Myers, M. N.; Martin, M. *Anal. Chem.* **1979**, *51*, 30–33.
(14) Yau, W. W.; Kirkland, J. J. *Sep. Sci. Technol.* **1981**, *16*, 577–605.
(15) Wahlund, K.-G.; Winegarner, H. S.; Caldwell, K. D.; Giddings, J. C. *Anal. Chem.* **1986**, *58*, 573–578.
(16) Williams, P. S.; Kellner, L.; Beckett, R.; Giddings, J. C. *Analyst (London)* **1988**, *113*, 1253–1259.
(17) Carlshaf, A.; Jonsson, J. Å. *J. Chromatogr.* **1988**, *461*, 89–93.
(18) Litzén, A.; Wahlund, K.-G. *J. Chromatogr.* **1989**, *476*, 413–421.
(19) Kirkland, J. J.; Yau, W. W. *J. Chromatogr.* **1990**, *499*, 655–668.
(20) Chen, X.; Wahlund, K.-G.; Giddings, J. C. *Anal. Chem.* **1988**, *60*, 362–365.
(21) Giddings, J. C. *Unified Separation Science*; Wiley: New York, 1991.
(22) Giddings, J. C.; Chen, X.; Wahlund, K.-G.; Myers, M. N. *Anal. Chem.* **1987**, *59*, 1957–1962.
(23) Giddings, J. C.; Myers, M. N. *Sep. Sci. Technol.* **1978**, *13*, 637–645.
(24) Giddings, J. C. *J. Chem. Educ.* **1973**, *50*, 667–669.
(25) Giddings, J. C.; Caldwell, K. D. *Anal. Chem.* **1984**, *56*, 2093–2099.
(26) Giddings, J. C.; Kumar, V.; Williams, P. S.; Myers, M. N. In *Polymer Characterization: Physical Property, Spectroscopic, and Chromatographic Methods*; Advances in Chemistry Series 227; Craver, C. D., Provder, T., Eds.; American Chemical Society: Washington, DC, 1990; Chapter 1.
(27) Williams, P. S.; Giddings, J. C. *Anal. Chem.* **1987**, *59*, 2038–2044.
(28) Giddings, J. C. *Anal. Chem.* **1986**, *58*, 2052–2056.
(29) Koch, T.; Giddings, J. C. *Anal. Chem.* **1986**, *58*, 994–997.
(30) Giddings, J. C.; Moon, M. H.; Williams, P. S.; Myers, M. N. *Anal. Chem.* **1991**, *63*, 1366–1372.
(31) Dalas, E.; Koutsoukos, P.; Karalskakis, G. *Colloid Polym. Sci.* **1990**, *268*, 155–162.
(32) Peterson, R. E., II; Myers, M. N.; Giddings, J. C. *Sep. Sci. Technol.* **1984**, *19*, 307–319.
(33) Myers, M. N.; Giddings, J. C. *Powder Technol.* **1979**, *23*, 15–20.
(34) Giddings, J. C.; Myers, M. N.; Caldwell, K. D.; Pav, J. W. *J. Chromatogr.* **1979**, *185*, 261–271.
(35) Caldwell, K. D.; Nguyen, T. T.; Myers, M. N.; Giddings, J. C. *Sep. Sci. Technol.* **1979**, *14*, 935–946.
(36) Giddings, J. C. *Sep. Sci. Technol.* **1983**, *18*, 765–773.
(37) Schure, M. R.; Caldwell, K. D.; Giddings, J. C. *Anal. Chem.* **1986**, *58*, 1509–1516.
(38) Giddings, J. C. *Sep. Sci. Technol.* **1986**, *21*, 831–843.
(39) Giddings, J. C.; Li, S.; Williams, P. S.; Schimpf, M. E. *Makromol. Chem., Rapid Commun.* **1988**, *9*, 817–823.
(40) Ratanathanawongs, S. K.; Giddings, J. C. *J. Chromatogr.* **1989**, *467*, 341–356.
(41) Barman, B. N.; Myers, M. N.; Giddings, J. C. *Powder Technol.* **1989**, *59*, 53–63.
(42) Segré, G.; Silberberg, A. *J. Fluid Mech.* **1962**, *14*, 115–135.
(43) Segré, G.; Silberberg, A. *J. Fluid Mech.* **1962**, *14*, 136–157.
(44) Saffman, P. G. *J. Fluid Mech.* **1965**, *22*, 385–400.
(45) Cox, R. G.; Brenner, H. *Chem. Eng. Sci.* **1968**, *23*, 147–173.
(46) Ho, B. P.; Leal, L. G. *J. Fluid Mech.* **1974**, *65*, 365–400.
(47) Vasseur, P.; Cox, R. G. *J. Fluid Mech.* **1976**, *78*, 385–413.
(48) Williams, P. S.; Koch, T.; Giddings, J. C. *Chem. Eng. Commun.*, submitted for publication.
(49) Myers, M. N.; Giddings, J. C. *Anal. Chem.* **1982**, *54*, 2284–2289.
(50) Giddings, J. C.; Williams, P. S.; Beckett, R. *Anal. Chem.* **1987**, *59*, 28–37.
(51) Williams, P. S.; Giddings, J. C.; Beckett, R. *J. Liq. Chromatogr.* **1987**, *10*, 1961–1998.
(52) Williams, P. S. Personal communication, University of Utah, Jan 10, 1991.

RECEIVED for review February 5, 1991. Revised manuscript received October 1, 1991. Accepted October 7, 1991. This work was supported by Public Health Service Grant GM10851-33 from the National Institutes of Health.